Anticrossings in solid-state laser spectroscopy

A. Wokaun,* S. C. Rand,† R. G. DeVoe, and R. G. Brewer
IBM Research Laboratory, San Jose, California 95193
(Received 13 January 1981)

We report the first observation of anticrossings in solid-state laser spectroscopy. Measurements are performed on the 6105-Å zero-phonon transition $^3H_4(\Gamma_1) \leftrightarrow {}^1D_2(\Gamma_1)$ of Pr^{3+} in a $YAlO_3$ crystal at 2° K where both ground- and excited-state anticrossings appear. A perturbation theory of the anticrossing signal is derived from the wave equations of motion for a three-level quantum system subject to a static interaction V between two neighboring levels (1 and 2) while a laser field resonantly excites the inhomogeneously broadened $2 \leftrightarrow 3$ transition. Ground- and excited-state gyromagnetic ratios $\gamma_i (i = X, Y, Z)$ and the interactions V are obtained by fitting the observed anticrossings to a diagonalized hyperfine-spin Hamiltonian for $^{141}Pr^{3+}$ which includes second-order ligand field corrections in terms containing the electron orbital angular momentum. Under certain conditions, one anticrossing signal develops into a strongly modulated oscillation with a period of ~ 20 G, an unexpected feature which appears to be a nonlinear optical coherence effect. The influence of anticrossing state mixing on optical free-induction-decay observations is also discussed.

I. INTRODUCTION

The related phenomena of level crossing and anticrossing have proved to be important spectroscopic techniques in atomic physics and constitute an area which predates both optical pumping and lasers. In level crossing, the resonance fluorescence of a suitable pair of degenerate Zeeman levels exhibits spatial interference as an external magnetic field is slowly swept through zero field (Hanle effect[1]) or a crossing at nonzero field.[2] In anticrossing,[3,4] a pair of excited Zeeman levels are subject to a small static interaction, and when an applied magnetic field is swept, the levels first approach and then repel each other rather than cross, causing the emission intensity to vary.

Most level crossings[5] and anticrossings[6] are detected in spontaneous emission although some absorption studies in atoms and molecules have now been performed using laser sources. The signals can then show both a linear or nonlinear[7–11] dependence on laser intensity. A recent example is the optical Hanle effect,[12] a light-shift-induced zero-field level crossing.

With a few exceptions, optical measurements of level crossings and anticrossings in solids are almost nonexistent. One exception is the photon echo study of ruby[13] which reveals a remarkable variation in the decay behavior when the Zeeman levels are tuned through a level crossing region. A related case is the detection of anticrossings and cross relaxation effects in molecular crystals of photoexcited triplet states using microwave spectroscopy.[14]

In this article, we apply the level anticrossing technique to solid-state laser spectroscopy, choosing the impurity ion crystal Pr^{3+}:$YAlO_3$ as an example. Several anticrossing signals are observed by linear absorption for the Pr^{3+} zero phonon transition $^3H_4(\Gamma_1) \leftrightarrow {}^1D_2(\Gamma_1)$ where both ground- and excited-state anticrossings appear. In Sec. II, we derive an expression for the anticrossing linear absorption signal of a transition subject to strong inhomogeneous broadening. In Sec. III, the detailed form of the ^{141}Pr nuclear quadrupole and Zeeman interactions, which give rise to anticrossing, is treated by a numerical diagonalization routine. The utility of anticrossings in determining solid-state hyperfine parameters is discussed in Sec. IV. We also comment on an anomalous modulation of the anticrossing signal which appears when certain experimental conditions are satisfied, and finally, the effect of anticrossing on optical free-induction decay is discussed.

II. THEORY OF THE ANTICROSSING SIGNAL

In this section an expression for an optically detected anticrossing signal is derived. The predicted signal applies to the experimental configuration of Fig. 1 where the intensity of a laser beam is monitored after passing through a sample containing resonant Pr^{3+} impurity ions in a $YAlO_3$ host crystal. By application of an external dc magnetic field, certain pairs of Pr^{3+} states approach each other and then exhibit repulsion or anticrossing behavior (Figs. 2 and 3) due to the combined influence of hyperfine and Zeeman interactions. As the magnetic field is swept through the anticrossing region, the anticrossing states mix and under appropriate conditions produce a corresponding intensity variation in the transmitted beam. We wish

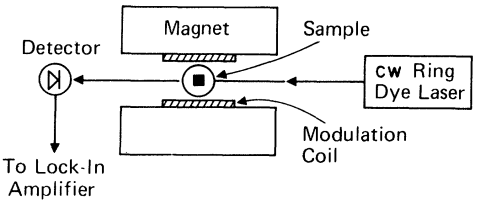

FIG. 1. Schematic of the experimental arrangement for detecting anticrossings.

to show, contrary to some discussions,[8,10,11] that anticrossings can be observed in absorption in solid-state laser spectroscopy even in the linear intensity regime. While nonlinear behavior is possible also, it is not essential.

For the purpose of this discussion assume the three-level quantum system of Fig. 4 where a laser field

$$\vec{E}_x(z,t) = \vec{e}_x E_0 \cos(\Omega t - kz) \tag{2.1}$$

resonantly excites the $1 \rightarrow 3$ or $2 \rightarrow 3$ transition and the states $|1\rangle$ and $|2\rangle$ anticross due to the perturbative interaction $\mathcal{H}_V$, the matrix element being

$$V = \langle 1|\mathcal{H}_V|2\rangle/\hbar \ . \tag{2.2}$$

The detailed form of this interaction will be considered in Sec. III. The total Pr^{3+} Hamiltonian

$$\mathcal{H} = \mathcal{H}_e + \mathcal{H}_V + \mathcal{H}_d + \mathcal{H}_0 \tag{2.3}$$

also contains an electronic component $\mathcal{H}_e$, a damping term $\mathcal{H}_d$ and the optical interaction

$$\mathcal{H}_0 = -\vec{\mu} \cdot \vec{E}_x(z,t) \ , \tag{2.4}$$

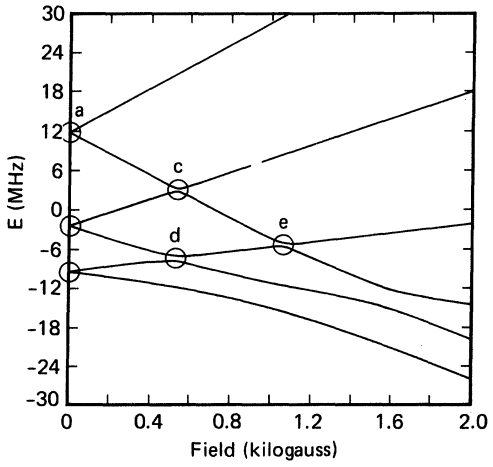

FIG. 2. Computer diagonalization of the $^{141}Pr^{3+}$ Zeeman-hyperfine Hamiltonian, Eq. (3.8), showing the ground-state $^3H_4(\Gamma_1)$ zero-field level crossing *a* and anticrossings *c*, *d*, and *e*. The parameters of Table I are utilized.

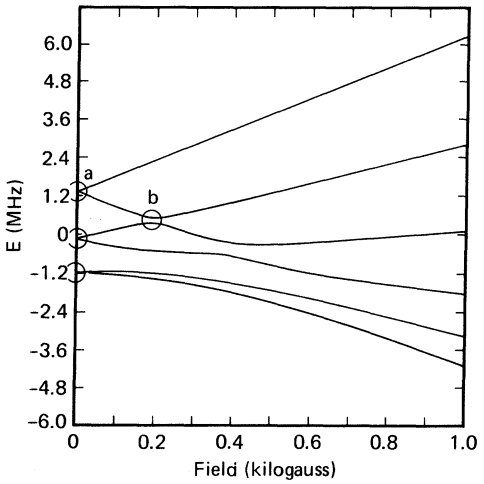

FIG. 3. Computer diagonalization of $^{141}Pr^{3+}$ Zeeman-hyperfine Hamiltonian, Eq. (3.8), showing the excited-state $^1D_2(\Gamma_1)$ zero-field crossings *a* and the anticrossing *b*.

where μ is the induced dipole and we assume that

$$\mathcal{H}_e >> \mathcal{H}_V >> \mathcal{H}_d > \mathcal{H}_0 \ . \tag{2.5}$$

We further assume that the two transitions $1 \rightarrow 3$ and $2 \rightarrow 3$ are strongly inhomogeneously broadened. Because of the perturbation $\mathcal{H}_V$, the two transitions are split, the minimum spacing being $2|V|$ as sug-

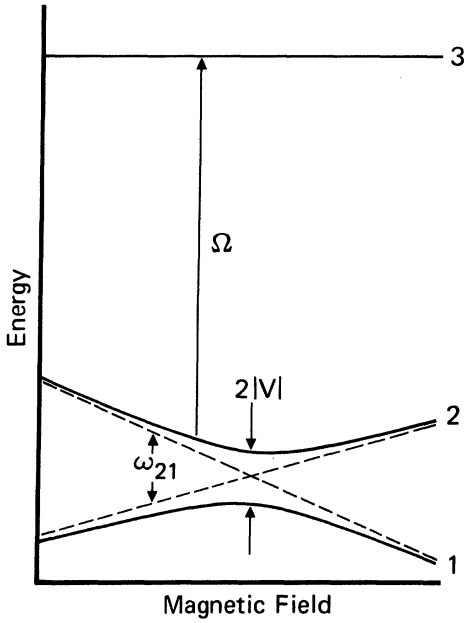

FIG. 4. Levels 1 and 2 exhibit anticrossing due to the interaction V where ω_{21} is the level splitting in the absence of an interaction ($V=0$). A light wave of frequency Ω resonantly excites the $2 \rightarrow 3$ transition and thus monitors the anticrossing tuning behavior as the magnetic field is swept. The quantities ω_{21}, V, and Ω are in angular units.

gested in Fig. 4. Because of the inequalities (2.5) and inhomogeneous broadening, the laser field excites one packet in the $1 \rightarrow 3$ transition and a second packet in the $2 \rightarrow 3$ transition. Hence, a single packet is not excited simultaneously in both transitions as in a double-resonance experiment. This situation affords a simplification allowing the two transitions to be treated independently in first approximation.

We seek a solution to the wave equation

$$i\hbar \frac{\partial \psi}{\partial t} = H\psi$$

of the form

$$\psi(t) = c_1(1)e^{-i\omega_1 t}|1\rangle + c_2(t)e^{-i\omega_2 t}|2\rangle + c_3(t)e^{-i\omega_3 t}|3\rangle \ .$$

Considering first the $2 \rightarrow 3$ transition, the equations of motion are

$$\dot{c}_1 = -\frac{\Gamma_1}{2}c_1 - iVe^{-i\omega_{21}t}c_2 \ , \tag{2.6a}$$

$$\dot{c}_2 = -\frac{\Gamma_2}{2}c_2 - iV^*e^{i\omega_{21}t}c_1 + \frac{i\chi_2}{2}e^{-i(\Delta t+kz)}c_3 \ , \tag{2.6b}$$

$$\dot{c}_3 = -\frac{\Gamma_3}{2}c_3 + i\frac{\chi_2}{2}e^{i(\Delta t+kz)}c_2 \ . \tag{2.6c}$$

The rotating-wave approximation has been applied; the zero-order eigenenergies are

$$\langle j|\mathcal{H}_e|j\rangle = \hbar\omega_j \text{ and } \omega_{ij} = \omega_i - \omega_j \ , \tag{2.7}$$

the Rabi frequencies for the 1-3 and 2-3 transitions are

$$\chi_1 = \mu_{13}E_0/\hbar = |\langle 1|\mathcal{H}_0|3\rangle|/\hbar \ ,$$
$$\chi_2 = \mu_{23}E_0/\hbar = |\langle 2|\mathcal{H}_0|3\rangle|/\hbar \ , \tag{2.8}$$

and the diagonal damping rates are given by

$$-\frac{i\hbar}{2}\Gamma_j = \langle j|\mathcal{H}_d|j\rangle \ . \tag{2.9}$$

Furthermore, the tuning parameter

$$\Delta = -\Omega + \omega_{32} + \alpha \text{ for } \omega_3 >> \omega_2 > \omega_1 \ , \tag{2.10}$$

where α is the shift in the Pr^{3+} transition frequency ω_{32} due to an inhomogeneity in the local crystalline Stark field. When the energy levels of Fig. 4 are inverted, the counter rotating field component is resonant and Eq. (2.10) becomes

$$\Delta = \Omega + \omega_{32} + \alpha \text{ for } \omega_2 > \omega_1 >> \omega_3 \tag{2.11}$$

and we replace in Eq. (2.6) $e^{\pm ikz}$ by $e^{\mp ikz}$.

A set of equations similar to Eq. (2.6) is obtained for the transition $1 \rightarrow 3$ by the index interchange $1 \leftrightarrow 2$. We see that three wave equations of motion offer a simplification over the nine equations of motion arising in a density-matrix treatment, but some generality is lost due to the absence of damping in the off-diagonal terms.

The two packets corresponding to the $1 \rightarrow 3$ and $2 \rightarrow 3$ transitions generate a field amplitude signal

$$E_s(z,t) = [\tilde{E}_{13}(z,t) + \tilde{E}_{23}(z,t)]e^{i(\Omega t-kz)} + \text{c.c.} \ , \tag{2.12}$$

which obeys Maxwell's wave equation

$$\frac{\partial \tilde{E}_{ij}}{\partial z} = -2\pi ikN\mu_{ij}\langle\langle\tilde{\rho}_{ij}(t)\rangle_{t_0}\rangle_I \qquad (ij = 13, 23) \tag{2.13}$$

for an optically thin sample of length L. Here, the slowly varying part $\tilde{\rho}_{ij}$ of the density matrix $\rho_{ij} = c_i c_j^*$ is defined by

$$\rho_{ij}(z,t) = \tilde{\rho}_{ij}(t)e^{i(\Omega t-kz)} \quad (ij = 13, 23) \tag{2.14}$$

and N is the Pr^{3+} atomic number density. Because we are interested in steady-state solutions of Eq. (2.6), the inner bracket of Eq. (2.13) performs the average

$$\langle\tilde{\rho}_{ij}(t)\rangle_{t_0} = K\int_{-\infty}^{t}\tilde{\rho}_{ij}(t-t_0)\,dt_0 \tag{2.15}$$

over all times t_0 that Pr^{3+} ions enter the absorbing levels i or j and thus commence absorbing laser light. The constant K is the rate that ions enter the absorbing state, due either to optical spontaneous emission or other forms of relaxation.

The outer bracket of Eq. (2.13) performs the average

$$\langle\tilde{\rho}_{ij}(\Delta)\rangle_I = \int_{-\infty}^{\infty}G(\Delta)\tilde{\rho}_{ij}(\Delta)\,d\Delta \tag{2.16}$$

over the Pr^{3+} inhomogeneous line-shape function

$$G(\alpha) = \frac{1}{\sqrt{\pi}\sigma}e^{-(\alpha/\sigma)^2} \ , \tag{2.17}$$

which is assumed to be Gaussian with $\Delta = \pm\Omega + \omega_{32} + \alpha$ corresponding to Eqs. (2.10) or (2.11).

In an experiment, the observable is the square of the total field,

$$\langle E_T^2\rangle_{\text{av}} = \langle|E_s + E_x|^2\rangle_{\text{av}} \ , \tag{2.18}$$

where the signal field E_s and the laser field E_x are given by Eqs. (2.12) and (2.1) and $\langle\ \rangle_{\text{av}}$ denotes a time average over an optical period. Equation (2.18) contains the cross term

$$I_s = 2E_0\text{Re}(\tilde{E}_{13} + \tilde{E}_{23}) \ , \tag{2.19}$$

which is the desired signal intensity where Re specifies the real part.

It now remains to evaluate $\tilde{E}_{13} + \tilde{E}_{23}$. We solve Eq. (2.6) by iteration using the Laplace transform method.[15] First, the wave equation is solved in first

order by neglecting the optical interaction $\mathcal{H}_0$. With the transformation $c(z)=\int_0^\infty c(t)e^{-zt}dt$, Eqs. (2.6a) and (2.6b) become

$$(z+\Gamma_1/2)c_1^{(1)}(z)=c_1(0)-iVc_2^{(1)}(z+i\omega_{21}) \ , \quad (2.20a)$$

$$(z+\Gamma_2/2)c_2^{(1)}(z)=c_2(0)-iV^*c_1^{(1)}(z-i\omega_{21}) \ , \quad (2.20b)$$

where the poles are

$$z_1^{(1)}=\tfrac{1}{2}[i\omega_{21}-\tfrac{1}{2}(\Gamma_2+\Gamma_1)] +\tfrac{1}{2}[i\omega_{21}+\tfrac{1}{2}(\Gamma_2-\Gamma_1)^2-4|V|^2]^{1/2} \ , \quad (2.21a)$$

$$z_2^{(1)}=\tfrac{1}{2}[i\omega_{21}-\tfrac{1}{2}(\Gamma_2+\Gamma_1)] -\tfrac{1}{2}[i\omega_{21}+\tfrac{1}{2}(\Gamma_2-\Gamma_1)^2-4|V|^2]^{1/2} \ , \quad (2.21b)$$

and $c_{1,2}(0)$ specify the initial conditions at $t=0$. Equations (2.20) yield

$$c_1(z-i\omega_{21})=\frac{(z+\Gamma_2/2)c_1(0)-iVc_2(0)}{(z-z_1)(z-z_2)} \ ,$$

$$c_2(z)=\frac{(z-i\omega_{21}+\Gamma_1/2)c_2(0)-iV^*c_1(0)}{(z-z_1)(z-z_2)} \ . \quad (2.22)$$

By the inverse transform

$$c(t)=\frac{1}{2\pi i}\int_{-i\infty+r}^{i\infty+r}e^{zt}c(z)\,dz \ ,$$

Eq. (2.22) reduces to the first-order solutions

$$c_1^{(1)}(t)=\frac{e^{-i\omega_{21}t}}{z_1-z_2}\{[(z_1+\Gamma_2/2)c_1(0)-iVc_2(0)]e^{z_1t}-[(z_2+\Gamma_2/2)c_1(0)-iVc_2(0)]e^{z_2t}\} \ , \quad (2.23a)$$

$$c_2^{(1)}(t)=\frac{1}{z_1-z_2}\{[(\Gamma_1/2+z_1-i\omega_{21})c_2(0)-iV^*c_1(0)]e^{z_1t}-[(\Gamma_1/2+z_2-i\omega_{21})c_2(0)-iV^*c_1(0)]e^{z_2t}\} \ . \quad (2.23b)$$

The above derivation simplifies somewhat with the realistic assumption that

$$\Gamma_1=\Gamma_2\equiv\Gamma \ .$$

The poles then become

$$z_1^{(1)}=-\frac{\Gamma}{2}+\frac{i}{2}[\omega_{21}+(\omega_{21}^2+4|V|^2)^{1/2}] \ ,$$

$$z_2^{(1)}=-\frac{\Gamma}{2}+\frac{i}{2}[\omega_{21}-(\omega_{21}^2+4|V|^2)^{1/2}] \ , \quad (2.24)$$

and Eq. (2.23) assumes the form

$$c_1^{(1)}(t)=\frac{ie^{-i\omega_{21}t}}{z_1-z_2}(me^{z_1t}+ne^{z_2t}) \ , \quad (2.25a)$$

$$c_2^{(1)}(t)=\frac{i}{z_1-z_2}(pe^{z_1t}+qe^{z_2t}) \ , \quad (2.25b)$$

where

$$m=ac_1(0)-vc_2(0), \quad n=-bc_1(0)+Vc_2(0) \ ,$$

$$p=-[V^*c_1(0)+bc_2(0)], \quad q=V^*c_1(0)+ac_2(0) \ ,$$

$$a=\tfrac{1}{2}[\omega_{21}+(\omega_{21}^2+4|V|^2)^{1/2}] \ , \quad (2.26)$$

$$b=\tfrac{1}{2}[\omega_{21}-(\omega_{21}^2+4|V|^2)^{1/2}] \ .$$

Note that the wave functions (2.23) agree identically with Wieder and Eck[4] who derived the transition probability for the case of spontaneous emission of the anticrossing levels 1 and 2.

We treat the case of absorption for inhomogeneously broadened transitions by formally integrating Eq. (2.6c), obtaining the second-order result

$$c_3^{(2)}(t)=e^{-\Gamma_3t/2}\left[c_3^{(2)}(0)+\frac{i\chi}{2}e^{ikz}\int_0^t c_2^{(1)}(t')e^{(i\Delta+\Gamma_3/2)t'}\,dt'\right] \quad (2.27)$$

in terms of the first-order solution $c_2^{(1)}(t)$. Substituting Eq. (2.25b) into Eq. (2.27) allows us to evaluate the bilinear product

$$c_3(t)c_2^*(t)=\rho_{32}(t)=\tilde{\rho}_{32}(t)e^{i(\Omega t-kz)} \ , \quad (2.28)$$

and the superscripts are now dropped. Performing the time average (2.15) of the slowly varying component $\tilde{\rho}_{32}$, we obtain

$$\langle\tilde{\rho}_{32}(t)\rangle_{t_0}=\frac{i\chi K}{2|z_1-z_2|^2}\left[\frac{-p}{i\Delta+\Gamma_3/2+z_1}\left(\frac{p^*}{-i\Delta-\Gamma_3/2+z_1^*}+\frac{q^*}{-i\Delta-\Gamma_3/2+z_2^*}\right)\right.$$
$$-\frac{q}{i\Delta+\Gamma_3/2+z_2}\left(\frac{p^*}{-i\Delta-\Gamma_3/2+z_1^*}+\frac{q^*}{-i\Delta-\Gamma_3/2+z_2^*}\right)$$
$$\left.+\frac{1}{i\Delta+\Gamma_3/2+z_1}\left(\frac{pp^*}{z_1+z_1^*}+\frac{pq^*}{z_1+z_2^*}\right)+\frac{1}{i\Delta+\Gamma_3/2+z_2}\left(\frac{p^*q}{z_1^*+z_2}+\frac{qq^*}{z_2+z_2^*}\right)\right] \ , \quad (2.29)$$

where it is assumed that the coherent preparation terms $c_3(0)c_2^*(0)=0$ and $c_3(0)c_1^*(0)=0$.

To average Eq. (2.29) over the inhomogeneous line shape, we apply Eq. (2.16) evaluating the integrals by contour integration under the assumption that the Gaussian is slowly varying and can be factored outside the integral when $\sigma >> (\Gamma^2+4|V|^2)^{1/2}$. Consider first that the three states are ordered in energy according to Eq. (2.11) so that the decay rates of lower and upper states satisfy $\Gamma_3 < \Gamma$. Then the poles of $1/(i\Delta+\Gamma_3/2+z_{1,2})$ in Eq. (2.29) reside in the lower half plane (lhp) while the remaining poles lie in the upper half plane (uhp). When the level structure is inverted satisfying Eq. (2.10), we similarly assume that $\Gamma < \Gamma_3$ and then all poles are in the uhp. In either case, we find that

$$\langle\langle\tilde{\rho}_{32}(t)\rangle_{t_0}\rangle_I = \frac{-i\pi\chi_2 G(|\omega_{32}|-\Omega)K}{2(\omega_{21}^2+4|V|^2)} \times\left[\frac{2|V|^2c_1^2(0)+(\omega_{21}^2+2|V|^2)c_2^2(0)}{\Gamma}+\frac{2\Gamma|V|^2[c_2^2(0)-c_1^2(0)]}{\omega_{21}^2+\Gamma^2+4|V|^2}\right] . \tag{2.30}$$

For the $1\leftrightarrow 3$ transition, the quantity $\langle\langle\tilde{\rho}_{31}(t)\rangle_{t_0}\rangle_I$ is derived from Eq. (2.30) by the index interchange $1\leftrightarrow 2$.

A trivial integration of Eq. (2.13) for both transitions, $1\leftrightarrow 3$ and $2\leftrightarrow 3$, yields the linear absorption anticrossing signal (2.19)

$$I_s=-2\pi^2 kNL\hbar GK\left[\frac{c_1^2(0)\chi_1^2+c_2^2(0)\chi_2^2}{\Gamma}+\frac{2|V|^2}{\Gamma(\omega_{21}^2+\Gamma^2+4|V|^2)}(\chi_1^2-\chi_2^2)[c_2^2(0)-c_1^2(0)]\right] , \tag{2.31}$$

where it is assumed that

$$G(|\omega_{32}|-\Omega)\sim G(|\omega_{31}|-\Omega)\equiv G .$$

As the level splitting ω_{21} is tuned, the first term of Eq. (2.31) remains invariant and provides a constant background signal whereas the second term displays anticrossing behavior in the form of a Lorentzian line shape of angular linewidth

$$\Delta\omega_{1/2}=(\Gamma^2+4|V|^2)^{1/2} . \tag{2.32}$$

We now see that the anticrossing signal vanishes when either the dipole matrix elements or the population difference of the anticrossing states satisfy

$$\chi_1^2-\chi_2^2=0 \quad \text{or} \quad c_2^2(0)-c_1^2(0)=0 . \tag{2.33}$$

This occurs even though the wave-function admixture of the anticrossing states varies as ω_{21} is tuned because the gain of light intensity in one transition is just lost by the other. However, linear absorption anticrossing signals can be detected in systems such as Pr^{3+}:LaF_3 or Pr^{3+}:$YAlO_3$ due to the fact that Eq. (2.33) is often violated, i.e., $\chi_1^2\neq\chi_2^2$ and optical pumping redistributed the population among the Zeeman substrates so that $c_2^2(0)\neq c_1^2(0)$. This conclusion seems to disagree with earlier work which states that linear absorption anticrossing signals vanish for inhomogeneously broadened transitions.[8,10,11]

In contrast to anticrossing signals detected by spontaneous emission, the absorption signal predicted by Eq. (2.31) is equally valid for anticrossings in lower and upper transition states, consistent with Eqs. (2.10) and (2.11).

In addition, the anticrossing term goes to zero in the limit $V\rightarrow 0$, and therefore Eq. (2.31) does not apply to level crossing which requires that $V=0$. This result is expected since Eq. (2.31) fails when $4|V|^2<\Gamma^2$ as then the two transitions $1\rightarrow 3$ and $2\rightarrow 3$ are coupled and cannot be treated separately.

III. HAMILTONIAN: ZEEMAN AND QUADRUPOLE INTERACTIONS

To predict the magnetic field dependence of anticrossings of Pr^{3+}:$YAlO_3$ in the $^3H_4(\Gamma_1)$ and $^1D_2(\Gamma_1)$ states, it is necessary to diagonalize the Hamiltonian[16,17]

$$\mathcal{H}'=g\beta\vec{B}\cdot\vec{I}+a_J\vec{J}\cdot\vec{I}-g_N\beta_N\vec{B}\cdot\vec{I} +P[I_{Z'}^2-\tfrac{1}{3}I(I+1)+\tfrac{1}{3}\eta(I_{X'}^2-I_{Y'}^2)] . \tag{3.1}$$

which we treat as a perturbation on the ligand field interaction. The first term describes the Zeeman interaction of a Pr^{3+} ion with angular momentum $J\hbar$; the second term is the magnetic hyperfine interaction of ^{141}Pr with nuclear angular momentum $I\hbar$ where $I=\frac{5}{2}$; and the third term is the nuclear Zeeman interaction. The remaining terms are the nuclear electric quadrupole interaction where P is the quadrupole coupling constant and the asymmetry parameter $\eta=(V_{X'X'}-V_{Y'Y'})/V_{Z'Z'}$ is given in terms of the diagonal tensor components of the electric field gradient at the nucleus in the principal axis system (X',Y',Z').

Following Teplov,[16] we expand Eq. (3.1) in the principal axis system (X,Y,Z) of a pseudoquadrupole tensor Λ_{ii}, defined below, so that

$$\mathcal{H}'=\sum_{i=X,Y,Z}[g\beta(B_iJ_i)+a_J(J_iI_i)-g_N\beta_N(B_iI_i)] +P[I_{Z'}^2-\tfrac{1}{3}I(I+1)+\tfrac{1}{3}\eta(I_{X'}^2-I_{Y'}^2)] \tag{3.2}$$

derive the second-order eigenenergy correction

$$W^{(2)} = -\sum_{n\neq 0} \frac{|\langle n|\mathcal{H}'|0\rangle|^2}{\epsilon_n - \epsilon_0} , \tag{3.3}$$

where $|0\rangle$ and $\langle n|$ represent the lowest state and an excited state of a crystal-field Stark split manifold. The only nonvanishing matrix elements of Eq. (3.3) are those involving the electron angular momentum operators $J_{X,Y,Z}$ which appear in the first two terms of Eq. (3.2). We thus obtain

$$W^{(2)} = -\sum_{i=X,Y,Z} \left[2g\beta(B_i I_i) + \frac{(g\beta B_i)^2}{a_J} + a_J I_i^2 \right] \Lambda_{ii} , \tag{3.4}$$

where only the diagonal terms

$$\Lambda_{ii} = \sum_{n\neq 0} \frac{a_J |\langle 0|J_i|n\rangle|^2}{\epsilon_n - \epsilon_0} \tag{3.5}$$

survive in the principal axis system (XYZ). In Eq. (3.4), the first term is a linear Zeeman term which produces an enhanced ^{141}Pr nuclear magnetism,[16,17] and the second term is the quadratic Zeeman effect or Van Vleck paramagnetism. The third term is a pseudoquadrupole interaction[16,17] that can be cast in the form

$$-\sum_{i=X,Y,Z} a_J I_i^2 \Lambda_{ii} = D_a[I_Z^2 - \tfrac{1}{3}I(I+1)] + E_a(I_X^2 - I_Y^2) , \tag{3.6a}$$

where

$$D_a = a_J[(\Lambda_{XX} + \Lambda_{YY})/2 - \Lambda_{ZZ}] , \tag{3.6b}$$

$$E_a = \frac{a_J}{2}(\Lambda_{YY} - \Lambda_{XX}) . \tag{3.6c}$$

Teplov's Hamiltonian assumes that the Pr^{3+} ion is in a crystal field of orthorhombic symmetry. This symmetry is sufficiently high that all tensors, such as the pseudoquadrupole tensor Λ_{ij} and the field gradient tensor V_{ij}, can be diagonalized in the same principal axis system, making the above coordinate systems (XYZ) and $(X'Y'Z')$ coincident. For the case of Pr^{3+}:$YAlO_3$, the site symmetry C_{1h} is lower, and rigorously it is no longer always possible to diagonalize Λ_{ij} and V_{ij} in the same coordinate system. This can be seen by first selecting a coordinate system (XYZ) for the C_{1h} symmetry-adapted wave functions[18]

$$|J,\Gamma_1\rangle = \sum_{J_Z \text{ even}} a_{J_Z}|J,J_Z\rangle ,$$

$$|J,\Gamma_2\rangle = \sum_{J_Z \text{ odd}} a_{J_Z}|J,J_Z\rangle ,$$

which is coincident with that of the principal axes $(X'Y'Z')$ of the field gradient tensor V_{ii}. Here, $|J,J_Z\rangle$ is the spherical harmonic Y_{J,J_Z}. Now off-diagonal terms Λ_{ij} appear in Eq. (3.4) because the coefficients a_{J_Z}, which are unknown for Pr^{3+}:$YAlO_3$, are not restricted by symmetry. Of course, when when the coordinates (XYZ) are selected so that Λ_{ij} is diagonal, we recover Eq. (3.4) but then (XYZ) and $(X'Y'Z')$ are no longer coincident. The reflection operation of C_{1h} only specifies that the coordinate systems (XYZ) and $(X'Y'Z')$ be coincident in one principal axis while the other two axes are related by a rotation.[18a]

A simplification results, however, when we recog-

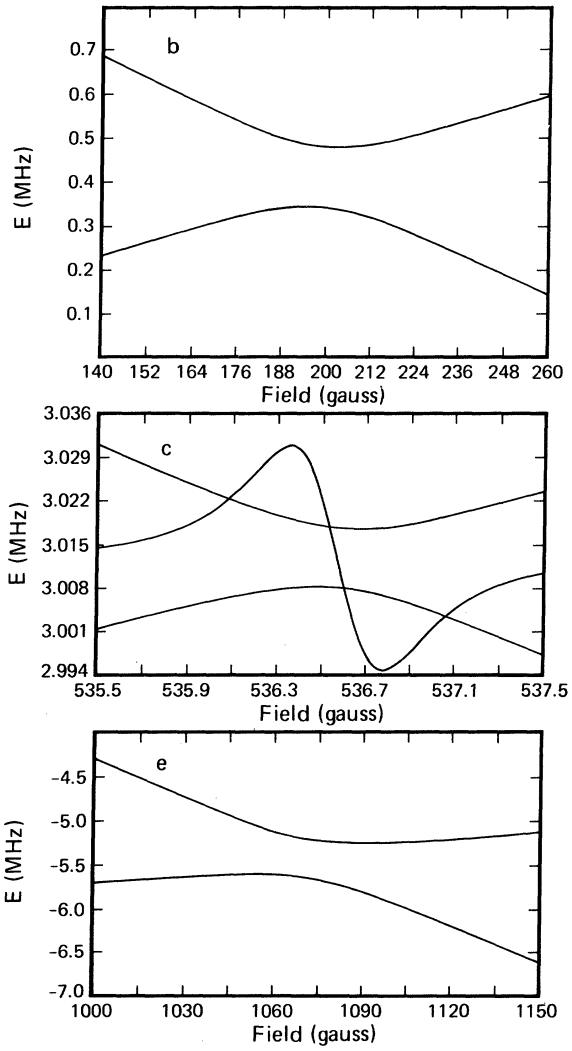

FIG. 5. Blowups of the anticrossings *b*, *c*, and *e* of Figs. 2 and 3 where the gap spacing or interaction $|V|$, listed in Table II, is more clearly shown. The anticrossing *c* shows a Lorentzian line shape signal in derivative form which is derived from Eq. (4.1); the peak-to-peak linewidth of ~0.4 G, which utilizes the parameters of Table I, does not explain the observed width of ~10 G as discussed in the text.

TABLE I. Hyperfine parameters of Pr^{3+}:$YAlO_3$ for $^3H_4(\Gamma_1)$ and $^1D_2(\Gamma_1)$.

	$^3H_4(\Gamma_1)$	$^1D_2(\Gamma_1)$
$\lvert D\rvert$ (MHz)	3.5255 ±0.0006[a]	0.3899 ±0.0057[a]
$\lvert E\rvert$ (MHz)	0.032 ±0.008[a]	0.0824 ±0.0040[a]
$\gamma_Z/2\pi$ (kHz/G)	11.910 ±0.10	2.50 ±0.5
$(\gamma_Y=\gamma_X)/2\pi$ (kHz/G)	1.75 ±0.75	2.0 ±1.0

[a]L. E. Erickson, Phys. Rev. B 19, 4412 (1979).

nize that the Pr^{3+} pseudoquadrupole moment is expected to be larger than the pure quadrupole moment, $|D_a| >> |P|$. Then, the Λ_{ii} tensor is dominant and with little error we can assume that (XYZ) and $(X'Y'Z')$ are coincident. This approximation is well satisfied by the Pr^{3+} ground state $^3H_4(\Gamma_1)$ and less so by the excited state $^1D_2(\Gamma_1)$ as discussed in Sec. IV.

With Eqs. (3.4) and (3.6), Eq. (3.1) becomes

$$\mathcal{H}' = -\hbar \sum_{i=X,Y,Z} \gamma_i B_i I_i + D[I_Z^2 - \tfrac{1}{3}I(I+1)] + E(I_X^2 - I_Y^2) + \sum_{i=X,Y,Z} \frac{(g\beta B_i^2)\Lambda_{ii}}{a_J} , \quad (3.7a)$$

where

$$\gamma_i = (g_N\beta_N + 2g\beta\Lambda_{ii})/\hbar , \quad (3.7b)$$

$$D = D_a + P , \quad (3.7c)$$

$$E = E_a + \tfrac{1}{3}P\eta . \quad (3.7d)$$

Note that the g values as defined in Eq. (3.1) are positive and that the term $2g\beta\Lambda_{ii}$ of Eq. (3.7b) appears with a plus sign, in agreement with Bleaney[17] but not Teplov[16] or Erickson.[19] Since the hyperfine constant for $^{141}Pr^{3+}$ is positive, $a_J = +1093$ MHz,[17] it follows that $\Lambda_{ii} > 0$ and the enhancement of γ_N in Eq. (3.7b) is positive.

Considering only the linear Zeeman and quadrupole terms of Eq. (3.7a), we rewrite the components of the field B in polar coordinates and obtain

$$\mathcal{H}' = -B_0\hbar(\gamma_X I_X \sin\theta\cos\phi + \gamma_Y I_Y \sin\theta\sin\phi + \gamma_Z I_Z \cos\theta) + D[I_Z^2 - \tfrac{1}{3}I(I+1)] + E(I_X^2 - I_Y^2) . \quad (3.8)$$

The diagonalization of the 6×6 energy matrix arising from Eq. (3.8) assumes that the axis of quantization is along the principal Z axis and the operation

$$I_Z\psi = m\psi$$

defines the ^{141}Pr nuclear spin eigenvalue m. The off-diagonal matrix elements of Eq. (3.8) are gener-

TABLE II. Anticrossing position, linewidth, and $|V|$ of the Pr^{3+}:$YAlO_3$ transition $^3H_4(\Gamma_1) \leftrightarrow {}^1D_2(\Gamma_1)$.

Anticrossing	State	Angles α,γ (deg)	Field (G) Observed	Field (G) Calc.	Observed linewidth[a] (G)	$\lvert V\rvert/\pi$ (kHz)
a[b]	$^3H_4$, $^1D_2$	0,0	0	0	50	0
b	$^1D_2$	0,0	200	200	80	195
c	$^3H_4$	0,0	536.5	536.5	10	9.2
c[c]	$^3H_4$	0,0.9	524 550	524 550	7.8 7.8	9.2
d	$^3H_4$	0,0	535	530	105	866
e	$^3H_4$	0,0	1073	1073	120	442

[a]Peak to peak values of derivative line shape. Due to the field modulation, anticrossings a, b, d, and e are broadened by ~25 G while c is broadened by ~8 G.

[b]This is a zero-field level crossing rather than an anticrossing.

[c]Because of the γ rotation, two anticrossings appear corresponding to the two inequivalent Pr^{3+} sites.

ated by

$$I_X=\tfrac{1}{2}(I_+ + I_-) \ , \quad I_Y=\frac{1}{2i}(I_+ - I_-) \ ,$$

where

$$\langle m \pm 1|I_\pm|m\rangle = [(I \mp m)(I \pm m+1)]^{1/2}$$

The quadratic terms are given by

$$\langle m'|I_i^2|m\rangle = \langle m'|I_i|m''\rangle\langle m''|I_i|m\rangle \qquad (i=X,Y,Z)$$

where $m'=m$ for I_Z and $m'=m,m\pm2$ for $I_{X,Y}$. The results of this numerical calculation are shown in Figs. 2, 3, and 5 and Tables I and II.

IV. DETECTION OF ANTICROSSINGS

A. Experimental technique

Anticrossings are monitored with the experimental arrangement of Fig. 1 which assumes the $YAlO_3$ crystal geometry of Fig. 6. The beam of a single mode cw ring dye laser progagates along the c axis of a crystal of 0.1 at.% Pr^{3+}:$YAlO_3$, immersed in liquid helium at 1.8 K, and thereby resonantly excites the Pr^{3+} transition $^3H_4(\Gamma_1) \leftrightarrow {}^1D_2(\Gamma_1)$ at a wavelength of 610.5 nm. The laser field is polarized parallel to the crystal a axis, is focused slightly within the sample to a 200-μm diameter, and has a power in the range 10 to 80 mW. When an external dc magnetic field is applied to the crystal along the b axis and is slowly swept through an anticrossing, in the region 0 to 2 kG, the intensity of the transmitted beam changes. The magnitude of this change is typically 0.1% and is detected with a PIN diode (EGG-SGD160) using phase-sensitive detection. For this purpose, the magnetic field is modulated sinusoidally in the range 8 to 25 G peak to peak at a frequency of a few kilohertz, and the anticrossing signals are displayed as a derivative line shape on an XY chart recorder. Signals in quadrature were too small to be detected.

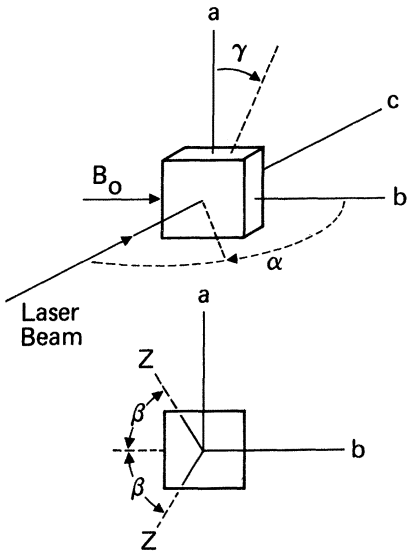

FIG. 6. In Zeeman studies, the $YAlO_3$ crystal is rotated either about the c axis through the angle γ or about the a axis through the angle α. When the angles $\alpha=0°$ and $\gamma=0°$, the magnetic field B_0 is parallel to the b axis and the laser beam propagates parallel to the c axis. For the $^3H_4(\Gamma_1)$ state, $\beta=56.50°$, and for the $^1D_2(\Gamma_1)$ state, $\beta=40°$ where the principal nuclear Z axes of the two inequivalent Pr^{3+} sites lie in the ab plane.

The space group of $YAlO_3$ is $D_{2h}^{16}=Pbnm$ and has an orthorhombic unit cell.[20] The yttrium ions are located in the two inequivalent sites, and the praseodymium ion substitutes for yttrium, retaining the orginal C_{1h} site symmetry. The crystal was cut and polished in the form of a platelet with dimensions $5\times5\times1.1$ mm^3 parallel to the crystal axes a:b:c. X-ray patterns confirm that the crystal axes are parallel to the faces as in Fig. 6 to an uncertainty of 1°. The crystal can be oriented in either of two orthogonal rotations, through the angles γ or α of Fig. 6, allowing the fixed Zeeman field to make various angles with the crystal axes. In this way, the angular dependence of the magnetic field position of the anticrossing signal can be determined and compared with theory.

The dc magnet (Varian V-4005) was calibrated with a Hall probe (Bell 640) which in turn was calibrated with a reference magnet (Varian 2100) locked to the proton NMR resonance at 23 MHz. In the range of these measurements, 0 to 2000 G, the field is known to an uncertainty of ±1%.

As noted previously for the case of Pr^{3+}:LaF_3, optical pumping depletes the population of the hyperfine packets which absorb laser light and reduces the signal to nondetectable levels.[21,22] As in the past,[21,22] we sweep the laser freqeuncy slowly at ~16 Mhz/msec so that the optical pumping process is partially reversed and a sizable population is maintained. Anticrossings were also detected in Pr^{3+}:LaF_3 but were not studied in the same detail as Pr^{3+}:$YAlO_3$.

B. Observations and results

Figure 7(b) is an example of anticrossings observed in Pr^{3+}:$YAlO_3$ for the case $\alpha=0°$ and $\gamma=0°$ where the signals appear as derivative line shapes with an intensity that varies approximately linearly with laser intensity. The first signal, labeled "a," is a zero-field level crossing and as the magnetic field increases, four anticrossings appear labeled b, c, d, and e. These five signals are in perfect agreement with the number predicted by the diagonalization cal-

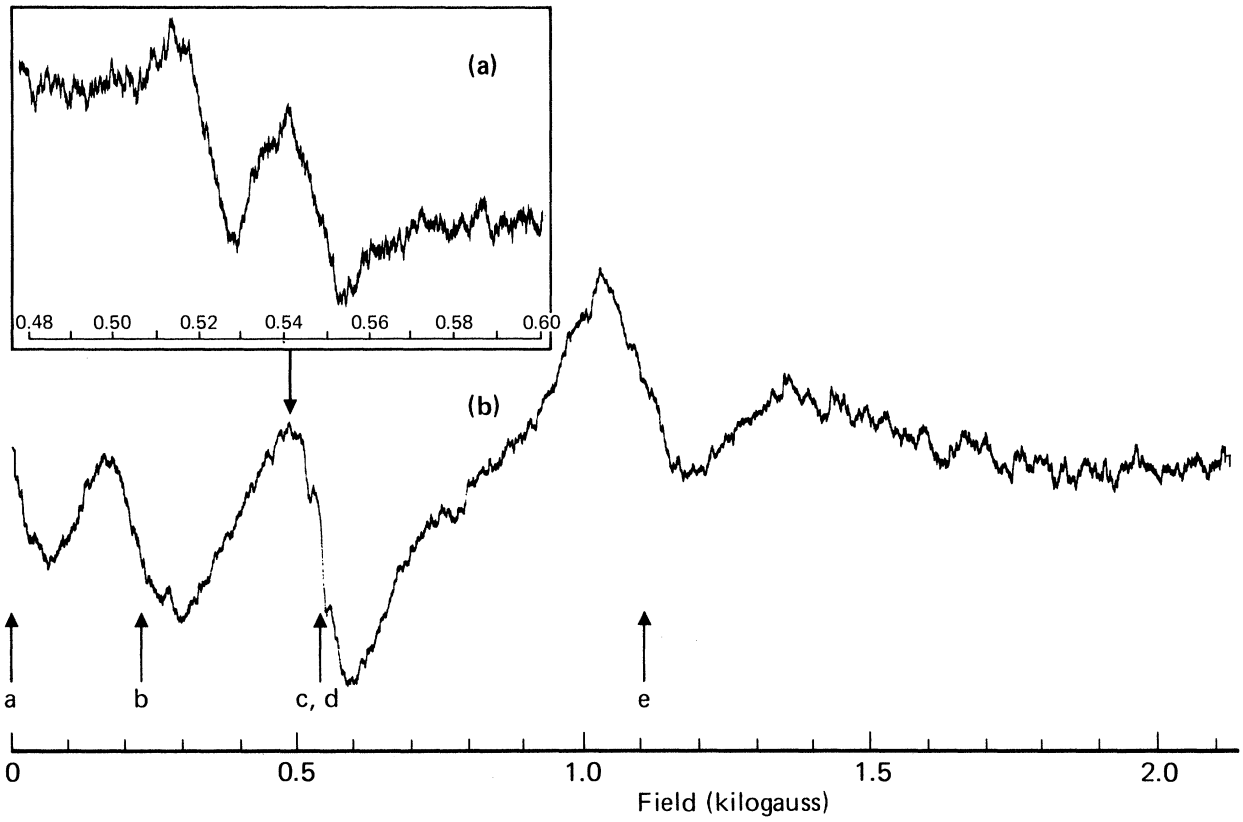

FIG. 7. Lower trace: Observed zero-field level crossing and anticrossings of 0.1 at.% Pr^{3+}:$YAlO_3$ at 2° K where the rotation angles are $\alpha=0°$, $\gamma=0°$. Upper trace: The sharp anticrossing c which rides on the broader d anticrossing splits into two well-resolved anticrossings when $\alpha=0°$, $\gamma=0.9°$ (see Table II). The scale is in kilogauss.

culations shown in Fig. 2 for $^3H_4(\Gamma_1)$ and in Fig. 3 for $^1D_2(\Gamma_1)$ where the features are labeled in the same way as in Fig. 7. The calculations assume the hyperfine parameters of Table I and allow us to identify that the b anticrossing occurs in the $^1D_2(\Gamma_1)$ excited state while the c, d, and e anticrossings occur in the $^3H_4(\Gamma_1)$ ground state. The characteristics of these anticrossings are summarized in Table II which gives the position of the anticrossing line, the linewidth, and the calculated minimum level spacing at the anticrossing expressed by a parameter $2|V|$. Note that since the exact diagonalization involves all states, V cannot be correlated rigorously with a matrix element just between two states as in Eq. (2.2).

The fact that the interaction V is nonzero (Table II) proves that features b through e are all anticrossings, i.e., as a pair of levels approach each other, they ultimately repel one another rather than cross. Group-theoretical arguments also predict this behavior. Since the symmetry of a general electric field gradient tensor ($\eta \neq 0$) is D_{2h} and the symmetry of the Zeeman interaction is the one-dimensional rotation group SU(1), the symmetry of the combined interaction is

$$D_{2h} \cap C_\infty = \begin{cases} C_2 \text{ if magnetic field is along a principal axis} \\ \{E\} \text{ otherwise} . \end{cases}$$

The group $\{E\}$ possesses no symmetry element beyond the identity operation so that all functions transform identically according to one irreducible representation and all basis states can mix or give rise to anticrossings. This is a manifestation of the noncrossing rule where states of the same symmetry do not cross. For the experiments reported here, only anticrossings are expected since the field never lies along a principal axis. Should the magnetic field lie along a principal axis, then the rotation operation $R_z(\phi)|m\rangle = e^{-im\phi}|m\rangle$ for C_2 symmetry ($\phi=\pi$) yields two groups of states $\{|\frac{5}{2}\rangle, |\frac{1}{2}\rangle, |-\frac{3}{2}\rangle\}$ and $\{|-\frac{5}{2}\rangle, |-\frac{1}{2}\rangle, |\frac{3}{2}\rangle\}$ which transform according to different irreducible representations. For this case, two eigenstates derived from the same group can anticross while two eigenstates derived from the two different symmetry groups can cross.

The tuning behavior of the anticrossing is dominat-

ed by the γ_Z term in the Hamiltonian since it gives rise to a first-order Zeeman effect. The γ_X and γ_Y terms, which we consider later, produce a small second-order Zeeman effect for fields 0 to 2000 G, and while these terms broaden the anticrossing line, they do not result in a noticeable shift of line center. The magnitude of γ_Z is determined from calculations, as shown in Fig. 5, which reproduce the observed line centers listed in Table II. For the $^3H_4(\Gamma_1)$ state, the calculation assumes Erickson's values[19] of the quadrupole parameters D and E and his determination that the principal Z axis of the quadrupole tensor lies in the crystal ab plane and at an angle $\beta = \pm 56.50°$ to the b axis (Fig. 6). It follows that for C_{1h} site symmetry the principal $X(Y)$ axis also lies in the ab plane while the $Y(X)$ axis is perpendicular to it. The resulting value $\gamma_Z/2\pi = 11.910 \pm 0.10$ kHz/G agrees well with Erickson's low-field-corrected value[19,23] 11.7 ± 0.04 kHz/G. The precision of our fit, as indicated in Table II, is uncertain by about 0.2% but the absolute error is of the order of $\pm 1\%$ due largely to the limiting signal-to-noise ratio and the uncertainty in the magnetic field.

The anticrossings also shift in a predictable manner when the $YAlO_3$ crystal is rotated about the a axis through the angle α or about the c axis through the angle γ (see Fig. 6). The angular dependence further corroborates the validity of the diagonalization routine, the choice of parameters, and the existence of two inequivalent Pr^{3+} sites. Figure 7(a) shows the pronounced effect of a small rotation of $\gamma = 0.9°$ ($\alpha = 0°$) on the sharp $^3H_4(\Gamma_1)$ anticrossing c which lies on top of the broader d anticrossing. This feature which is initially at 536.5 G when $\gamma = 0°$, splits into two components at 524 and 550 G corresponding to the two inequivalent Pr^{3+} sites indicated in Fig. 6. Table II shows that the calculations agree identically with these results.

In Fig. 8, the rotation angle α is varied ($\gamma = 0°$) where the observed anticrossing positions agree reasonably well with theory. When α becomes sufficiently large, the calculations reveal that the anticrossings are no longer distinct at which point signals cannot be detected.

For the $^1D_2(\Gamma_1)$ state, the orientation of the principal axis system is unknown although C_{1h} symmetry dictates that one principal axis must be perpendicular to a plane of symmetry, the ab plane. The α rotation pattern of Fig. 8 shows that the $^1D_2$ anticrossing b changes position very slowly with angle as do the $^3H_4$ anticrossings c and e and can be fitted approximately with the $^3H_4$ principal axis system indicated in Fig. 6. A more critical test is the γ rotation pattern where $\alpha = 0°$. We find that the b anticrossing splits into pairs of lines as follows: 200 G ($\gamma = 0°$), 240, 170 G ($\gamma = 10°$), and 310, 160 G ($\gamma = 20°$). This case can be fitted if the principal axis Z lies in the crystal ab plane as shown in Fig. 6 but $\beta = \pm 40°$, instead of $\pm 56.50°$, and $\gamma_Z(^1D_2)/2\pi = 2.5$ kHz/G. The twofold symmetry of the two inequivalent sites is required by the $YAlO_3$ crystal symmetry since one yttrium site can be transformed into the other by a glide plane.

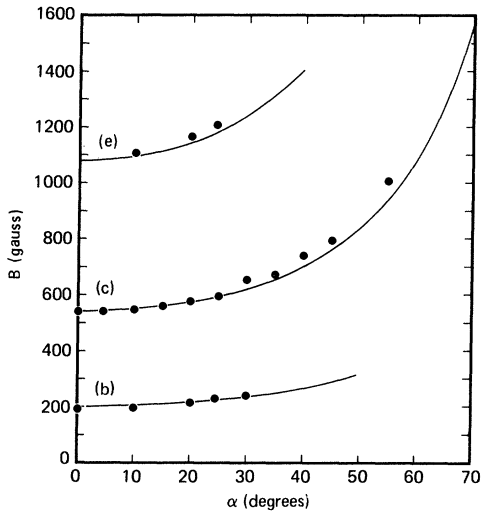

FIG. 8. Zeeman rotation pattern for the anticrossings b, c, and e where the angle α is varied and $\gamma = 0°$. Experiment: ●. Theory: ——.

In Table I, we note that the only splitting factor that is significantly enhanced is $\gamma_Z(^3H_4)$ as $\gamma_N/2\pi = 1.3$ kHz/G.

Equation (2.31) predicts that the anticrossing line shape is a Lorenztian of the form

$$I_s \sim \frac{1}{\omega_{21}^2 + 4|V|^2 + \Gamma^2} \ . \tag{4.1}$$

While the anticrossing line center is determined by γ_Z, the angular linewidth

$$\Delta\omega_{1/2} = (4|V|^2 + \Gamma^2)^{1/2}$$

can be determined by the effect of γ_X and γ_Y on the interaction $|V|$, i.e., one-half the minimum level spacing derived from the Hamiltonian (3.8). The observed linewidths of anticrossings b, d, and e given in Table II are strongly affected by $|V|$ since $4|V|^2 >> \Gamma^2$ where the population decay rates $\Gamma(^1D_2) = 5.4 \times 10^3$ sec^{-1} (Ref. 19) and $\Gamma(^3H_4) \leq 0.02$ sec^{-1}.[24] One wonders why the linewidth should be influenced by the static interaction V since Lorentzian line shapes are usually broadened by dynamic processes of a stochastic nature. The answer lies in the detection process. As the magnetic field is swept through the anticrossing region, the degree of mixing of the anticrossing states changes and consequently the transition probability for optical excitation changes correspondingly. Since the mixing process is confined to the region $|V|$, the optical response is also.

A fit of the linewidth is achieved by replacing $(\omega_{21}^2 + 4|V|^2)$ in Eq. (4.1) by the square of the

eigenenergy derived from the diagonalization routine and by varying the parameters γ_X and γ_Y. Indeed, this fit yields the minimum level spacing parameter $|V|$ given in Table II. Since the quadrupole parameter $E \sim 0$, it follows from Eqs. (3.5) and (3.6c) that $\gamma_X \sim \gamma_Y$. The resulting γ_X and γ_Y values are given in Table I and the interactions $|V|/\pi$ in Table II. The calculated peak to peak derivative linewidths for the *b*, *d*, and *e* anticrossings are 46, 100, and 52 G, respectively. The agreement with the observed widths is only suggestive. Instrumental limitations, such as the rf magnetic field modulation of 8 to 25 G, appear to mask the width of the narrow *c* anticrossing ($|V|/\pi = 9.2$ kHz) and the zero-field level crossing ($|V|/\pi = 0$), feature *a*, which cannot be explained by the $|V|$ or Γ terms in Eq. (4.1). Laser frequency jitter should have no effect on the linewidth measurements, and indeed, the anticrossing linewidths were unaffected by laser frequency locking.

C. Anomalous wiggle effect

In the region of the *c* and *d* anticrossings, an unexpected oscillation (Fig. 9) occurs when certain conditions are satisfied. First, the laser power must exceed 20 mW, and second, the laser frequency sweep rate must be at least 250 MHz/msec corresponding to a ±85 MHz sweep at a repetition rate of 1.5 kHz or higher. The period of oscillation is about 20 G and remains invariant to changes in laser power or sweep rate. However, the amplitude of oscillation is remarkably affected showing a quadratic dependence on laser intensity and a vanishing amplitude when the sweep rate falls below 0.75 kHz.

The 20-G interval appears to be unrelated to hyperfine or superhyperfine splittings or Rabi oscillations and is probably a nonlinear coherence phenomenon. Since the $^1D_2(\Gamma_1)$ radiative lifetime is 0.185 msec (Ref. 19) and the hyperfine splittings are of the order of a few megahertz, the laser frequency sweep is large enough to coherently prepare packets of three-level quantum systems (Fig. 4). Thus, the theory of Sec. II does not apply. The dynamics of coherent two-photon processes in three-level quantum systems has been investigated previously[25] for certain cases and suggests a quantum beat effect[26] which produces two sidebands shifted by the 1-2 level spacing $\sim 2|V|$. However, this is not an oscillation and the physical origin of these anticrossing oscillations remains mysterious.

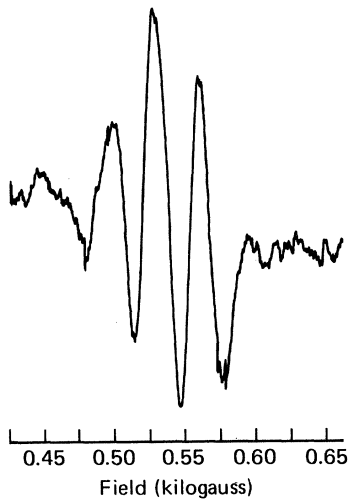

FIG. 9. Anomalous modulation effect in the region of anticrossings *c* and *d*. The laser frequency is swept through ±85 MHz at a repetition rate of 1.5 kHz and the cw laser power is 80 mW.

D. Optical free induction decay

Compaan *et al.*[13] have reported that the photon echo decay rate of the Cr^{3+} ion in ruby undergoes dramatic changes in the region of a level crossing. The effect is due to the mixing of Cr spin states which modifies its dipolar interaction with a surrounding Al nuclei. We were tempted, therefore, to see if the Pr^{3+}:$YAlO_3$ system exhibits a similar behavior in an anticrossing particularly since the anticrossing curves (Figs. 2 and 3) can exhibit a near zero slope causing the Pr^{3+} magnetic moment and its magnetic interactions to vanish.

Optical free-induction-decay (FID) measurements were conducted using the method of laser frequency switching a cw ring dye laser that is frequency locked to an external reference cavity.[22] For nonzero fields either on or off an anticrossing, the optical dephasing time is $T_2 = 76$ μsec, corresponding to a 2.1-kHz half-width at half maximum linewidth. Using the same experimental setup and a two-pulse laser frequency switching sequence with optical heterodyne detection, we find that the photon echo yields precisely the same dephasing time as the FID, to within a few percent uncertainty, in contrast to a previous report[27] which asserts that echoes and FID give different results. The absence of a change in the decay rate due to the anticrossing has two possible explanations. First, the FID signal arises from all possible optical transitions among the Zeeman substates whereas an anticrossing only involves one pair. This is a dilution effect. And second, the residual linewidth of 2.1 kHz might not be magnetic in origin. At present, it is not possible to decide which explanation prevails.

ACKNOWLEDGMENTS

We thank Marvin J. Weber for kindly loaning us the Pr^{3+}:$YAlO_3$ crystal used in this study. One of us (R.G.B.) benefited from stimulating conversations with Harold Wieder. The technical assistance of K. L. Foster is appreciated also. Work supported in part by the U.S. Office of Naval Research.

*Present address: Bell Telephone Laboratories, Holmdel, N.J. 07733.
†Present address: Dept. of Physics, Stanford University, Stanford, Calif. 94305.

[1]W. Hanle, Z. Phys. 30, 93 (1924).
[2]F. D. Colegrove, P. S. Franken, R. R. Lewis, and R. H. Sands, Phys. Rev. Lett. 3, 420 (1959); P. A. Franken, Phys. Rev. 121, 508 (1961).
[3]T. G. Eck, L. L. Foldy, and H. Wieder, Phys. Rev. Lett. 10, 239 (1963).
[4]H. Wieder and T. G. Eck, Phys. Rev. 153, 103 (1967).
[5]C. Cohen-Tannoudji, in *Frontiers in Laser Spectroscopy,* edited by R. Balian, S. Haroche, and S. Liberman (North-Holland, Amsterdam, 1977), p. 73; D. R. Crosley and R. N. Zare, Phys. Rev. Lett. 18, 942 (1967).
[6]G. W. Series, Phys. Rev. Lett. 11, 13 (1963); Phys. Rev. 136, A684 (1964).
[7]A. C. Luntz, R. G. Brewer, K. L. Foster, and J. D. Swalen, Phys. Rev. Lett. 23, 951 (1969); A. C. Luntz and R. G. Brewer, J. Chem. Phys. 53, 3380 (1970).
[8]K. Shimoda, Jpn. J. Appl. Phys. 11, 564 (1972).
[9]M. S. Feld, A. Sanchez, A. Javan, and B. J. Feldman, in *Proceedings of the Aussois Conference on High Resolution Molecular Spectroscopy,* edited by J. C. Pebay-Peyroula and J. C. Lehmann (CNRS, Paris, 1973), p. 87.
[10]J. Sakai and M. Katayama, Appl. Lett. 28, 119 (1976).
[11]T. Amano and R. H. Schwendeman, J. Mol. Spectrosc. 78, 437 (1979).
[12]V. P. Kaftandjian, C. Deslart, and J. C. Keller, Phys. Rev. A 23, 1365 (1981); P. A. Lakshmi and G. S. Agarwal, *ibid.* (in press).
[13]A. Compaan, L. Q. Lambert, and I. D. Abella, Opt. Commun. 3, 236 (1971); A. Compaan, Phys. Rev. B 11, 4450 (1972); L. Q. Lambert, *ibid.* 7, 1834 (1973).
[14]W. S. Veeman and J. H. Van der Waals, Chem. Phys. Lett. 7, 65 (1970); W. S. Veeman, A. L. J. Van der Poel, and J. H. Van der Waals, Mol. Phys. 29, 225 (1975); M. J. Hunt, A. L. Mackay, and D. R. Edmonds, Chem. Phys. Lett. 34, 473 (1975); G. Kothandaraman, P. F. Brode, III, and D. W. Pratt, *ibid.* 51, 138 (1977); A. Suisalu and P. Avarmaa, Phys. Status Solidi (b) 97, 69 (1980).
[15]A. Schenzle and R. G. Brewer, Phys. Rev. A 14, 1756 (1976).
[16]M. A. Teplov, Zh. Eksp. Teor. Fiz. 53, 1510 (1967) [Sov. Phys. JETP 26, 872 (1968)].
[17]B. Bleaney, Physica (Utrecht) 69, 317 (1973).
[18]C. J. Bradley and A. P. Cracknell, *The Mathematical Theory of Symmetry in Solids* (Clarendon, Oxford, 1972), Chap. II.
[18a]In general, the principal axes ($X''Y''Z''$) of the combined pure and pseudo quadrupole tensors will have one axis (the C_{1h} symmetry axis) in common with XYZ and $X'Y'Z'$, but the other two will be related by a rotation. When $|D_a|$ and $|P|$ are of comparable size, the difference between XYZ, $X'Y'Z'$, and $X''Y''Z''$ can affect the magnetic splitting. Let α be a rotation angle around the C_{1h} symmetry axis that transforms $X''Y''Z''$ into XYZ. Then the magnetic splitting term $\vec{B}\cdot\vec{\Lambda}\cdot\vec{I}$ in Eq. (3.4) can be transformed into the $X''Y''Z''$ system by a similarity transformation, where $\Lambda''=R^{-1}(\alpha)\Lambda R(\alpha)$. The resultant Λ'' tensor thus contains off-diagonal terms $\Lambda_{X''Y''}\neq 0$ but these do not contribute to the magnetic splitting in the first order. The diagonal terms of Λ'' become $\Lambda_{X''X''}=\Lambda_{XX}\cos^2\alpha+\Lambda_{YY}\sin^2\alpha$ and $\Lambda_{Y''Y''}=\Lambda_{YY}\cos^2\alpha+\Lambda_{XX}\sin^2\alpha$. A recent study of the $^1D_2$ magnetic splitting of Pr^{3+} in LaF_3 by R. M. Macfarlane and R. M. Shelby, Opt. Lett. 6, 96 (1981) assume that the Λ tensor has no off-diagonal elements, although the C_2 symmetry permits this and $|D_a|\sim|P|$. We estimated that the angle α can be as large as 30° for Pr^{3+} and LaF_3 although no measurements exist. The magnetic splittings they measure at very high magnetic fields, where the Hamiltonian is diagonalized in the XYZ axis system, can thus differ substantially from the low-field values, where the Hamiltonian is diagonalized along $X''Y''Z''$. Consequently, this comparison of their high-field g values with our low-field g values is not justified [R. G. DeVoe, A. Szabo, S. C. Rand, and R. G. Brewer, Phys. Rev. Lett. 42, 1560 (1979)].
[19]L. E. Erickson, Phys. Rev. B 19, 4412 (1979).
[20]S. Geller and E. A. Wood, Acta Crystallogr. 9, 563 (1956).
[21]A. Z. Genack, R. M. Macfarlane, and R. G. Brewer, Phys. Rev. Lett. 37, 1078 (1976); R. M. Macfarlane, A. Z. Genack, S. Kano, and R. G. Brewer, J. Lumin. 18/19, 933 (1979).
[22]R. G. DeVoe, A. Szabo, S. C. Rand, and R. G. Brewer, Phys. Rev. Lett. 42, 1560 (1979); S. C. Rand, A. Wokaun, R. G. DeVoe, and R. G. Brewer, *ibid.* 43, 1868 (1979).
[23]L. E. Erickson (private communication).
[24]We estimate $\Gamma(^3H_4)$ from the observed magnetic substate population recovery time.
[25]R. G. Brewer and E. L. Hahn, Phys. Rev. A 11, 1641 (1975).
[26]R. Haberkorn, H. L. Selzle, W. Dietz, S. H. Lin, and E. W. Schlag, Chem. Phys. 52, 363 (1980).
[27]R. M. Macfarlane, R. M. Shelby, and R. L. Shoemaker, Phys. Rev. Lett. 43, 1726 (1979).